Dynamics of a vibrating tip near or in intermittent contact with a surface

Ricardo García and Alvaro San Paulo

Instituto de Microelectrónica de Madrid, CSIC, Isaac Newton 8, 28760 Tres Cantos, Madrid, Spain

(Received 28 December 1999)

We discuss the stability of the tip motion in dynamic atomic force microscopy. A nonlinear dynamics analysis shows that the tip's phase space is divided in two basins of attraction. A phase space diagram dominated by either basin of attraction implies a stable motion while a substantial contribution from both basins is associated with instabilities. Because the dominance of a given basin of attraction depends on the tip-surface interaction potential and separation, stable and unstable motions are intrinsic features of an oscillating tip near or in intermittent contact with a surface.

The characterization and modification of surfaces at atomic and nanometer scales have experienced a radical transformation since the invention of scanning probe microscopes.[1] The control of the interaction forces, the precise monitoring of the tip-surface distance, and the potential for simultaneous topographic and compositional mapping of surfaces have made dynamic atomic force microscope (AFM) methods unique among nanometer-scale probes. High resolution images of DNA molecules and proteins,[2,3] true atomic resolution images of semiconductors and insulators,[4–6] and large scale patterning of materials[7] support the prominent role of dynamic force microscopy for atomic and nanometer scale characterization and manipulation of materials.

Martin, Williams, and Wickramasinghe explained the motion of a vibrating tip (cantilever) and its response to tip-surface forces in terms of a linear (harmonic) model.[8] The gradient of the force between tip and sample modifies the compliance of the cantilever, hence inducing a change in the oscillation amplitude due to the shift of the tip resonance, $\Delta\omega/\omega_0 = -\partial F/\partial z/2k_c$. The linear approximation has been improved and extended by several authors to consider the tip motion as described by a weakly disturbed harmonic oscillator.[9–11] In the process, linearized models have become the effective paradigm encompassing different dynamic AFM modes.

A few years ago, Gleyzes *et al.*[12] proposed that a vibrating scanning tunneling microscope (STM) tip close to a surface may show a bistable behavior when scanning the excitation frequency. Recently, several groups have explained the hysteresis effects observed in frequency sweeps and amplitude curves based on a bistable effect.[13–16] It has also been proposed that atomic resolution images in frequency modulation AFM are a direct consequence of the nonlinear behavior of the tip in the proximity of the sample surface.[17] A chaotic tip motion has also been predicted for systems with very high viscous damping.[18]

The generic dynamic properties of nonlinear systems with such complex features as bifurcations or chaotic attractors seems to be at odds with the predictable behavior expected for a sophisticated microscope. Here we study the stability of a dynamic force microscope based on a nonlinear dynamics analysis that gives rise to a phase space projection with two periodic attractors, i.e., the simultaneous existence of two steady-state oscillations. We also provide experimental data supporting the theoretical simulations.

The tip motion in dynamic AFM is approximately described by the differential equation

$$m\ddot{z} = -k_c z - \frac{m\omega_0}{Q}\dot{z} + F_{ts} + F_0\cos(\omega t), \tag{1}$$

where F_0 and ω are the amplitude and angular frequency of the driving force, respectively; Q, ω_0, and k_c are the quality factor, angular resonance frequency, and force constant of the free cantilever, respectively. The tip-surface interaction F_{ts} contains long range van der Waal forces and short range repulsive forces. Assuming additivity, for a sphere-flat geometry the van der Waals force is

$$F_{ts}(z_c, z) = -\frac{HR}{6d^2}, \tag{2}$$

where H is the Hamaker constant, R the tip radius, z_c the rest tip-surface separation, z the instantaneous tip position, and $d = z_c + z$. For separations $d < a_0$ [a_0 is an intermolecular distance that is introduced to avoid the divergence of Eq. (2)], the resulting van der Waals force is identified with the adhesion force of the Dejarguin-Muller-Toporov (DMT) theory.[19] In addition to the adhesion force, during the contact there are repulsive forces arising from Pauli and ionic repulsion. The repulsive force and the sample deformation are modeled by using the DMT theory,

$$F_{ts}(z_c, z) = -\frac{HR}{6a_0^2} + \bar{E}\sqrt{R}(a_0 - d)^{3/2}, \tag{3}$$

where $\bar{E}$ is the reduced elastic modulus of tip and sample. The numerical simulations were performed for R, $\omega = \omega_0$, k, Q, H, and $\bar{E}$ of 30 nm, 350 kHz, 40 N/m, 400, 6.4×10^{-20} J, and 1.51 GPa, respectively. The approximations used to derive above expressions as well as their justification can be found elsewhere.[15]

The equation that describes the tip motion is independent of the environment, however, the tip's final motion is sensitive to both tip-surface and the tip-environment interactions. Technical details of the operation of a dynamic AFM depend on the medium. Operation in air and liquids is usually performed with an amplitude modulation feedback (AM-AFM)

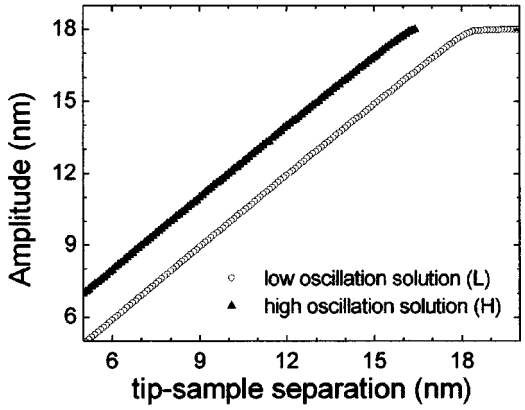

FIG. 1. Dependence of the high and low amplitude branches on the rest tip-surface separation. For $E=1.51$ GPa, A_H-A_L is almost independent on the separation.

while operation in vacuum requires a frequency modulation feedback. Here we focus our study on atmospheric pressure environments, i.e., AM-AFM systems with a Q factor between 50 and 1000. Nevertheless the results of this work are relevant to all methods that involve the oscillation of a tip at the proximity of a surface.

The numerical solution of Eq. (1) shows that for the range of free amplitudes (10–60 nm) used in AM-AFM and Young modulus above 0.1 GPa, the oscillation has two different solutions, a low (L) and high amplitude (H) solution, $z_{H(L)}=A_{H(L)}\cos(\omega t-\phi_{H(L)})$, respectively. Both of them are single period orbitals. For a hard-wall interaction potential, Eq. (1) is similar to the equation that describes the motion of impact oscillators.[20,21] Then, several stable states are predicted. However, the emergence of a large number of stable oscillations for a system with Q in the 50–1000 range requires amplitudes of several mm,[22] i.e., four to five orders of magnitude larger than those used in AM-AFM.

In Fig. 1, the dependence of the low and high oscillation branches on the rest tip-surface separation is plotted. Independent of the state, the amplitude decreases almost linearly with decreasing the separation. If the rest tip-surface separation and the external parameter F_0, remain unchanged, the initial conditions $(z,\dot{z},\omega t)$ will determine which state is reached. This plot illustrates an ambiguity in the operation of an amplitude modulation AFM. Both states could provide a value of the amplitude that matches the feedback amplitude A_{sp}. Even worse, because a given A_{sp} could be achieved for two different tip-surface separations, the tip could simply switch between one z_c position to the other rendering topographical images useless.

Figure 2 shows three snapshots $(t=0)$ of the phase space projection for different rest tip-surface separations. The phase space is divided in two interlocking regions. Initial conditions that give rise to the L state are plotted in gray, while those that give rise to the H state are plotted in white. A rotation of an angle ωt about the origin generates the phase space projection for a different time t. The Poincaré sections of H and L states are represented by circles.

For $z_c=16$ nm the basin of attraction of the low amplitude state dominates the phase space projection. At $z_c=14.5$ nm, the phase space is almost equally distributed between L and H basins of attraction, 52% and 48%, respectively. However, at $z_c=7.5$ nm, the H basin of attraction amounts to about 95% of the phase space projection. In the range of separations studied here, 6–18 nm, we find that the dependence of the phase space on the tip-surface separation can be divided into three regions. For z_c separations close to the value of the free amplitude, the phase space is dominated by the basin of attraction of the L state. Then there is an intermediate region where the phase space is roughly equally distributed between both basins of attraction. For z_c in the interval 6–12 nm, the phase space is dominated by the basin of attraction of the H state. The relative extension of the above regions depends on several factors such as the free

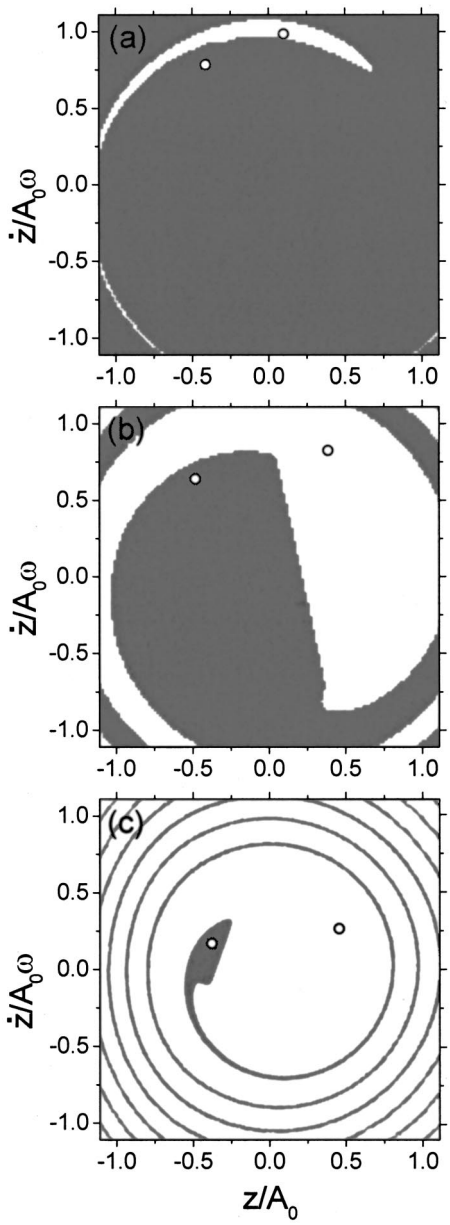

FIG. 2. Two-dimensional phase space projection for different tip-surface separations. The tip evolves from a phase space dominated by the basin of the low amplitude solution at $z_c=16$ nm (a), to a phase space with a balanced distribution of both basins of attraction at $z_c=14.5$ nm (b); at $z_c=7.5$ nm the phase space is dominated by the basin of the high amplitude solution (c). The open circles indicate the Poincaré sections of the H and L solutions. A_0 is the free oscillation amplitude.

amplitude, sample mechanical properties, dielectric constants, surface free energy, and the tip's radius.

The deterministic character of Eq. (1) implies that once a stable state is reached, the tip should oscillate indefinitely there. However, a perturbation could disturb the tip motion by introducing new initial conditions. Two kinds of perturbations can be considered in force microscopy, *extrinsic* and *intrinsic*. *Extrinsic* perturbations are those due to mechanical and thermal noise. Damping mechanisms have reduced mechanical noise to negligible levels in AFM. The contribution of the thermal noise to the tip motion can be evaluated following $\Delta z \sim \sqrt{(kT/k_c)}$ and $\Delta v \sim \Delta z \times \omega$.[23] For the case considered here, $\Delta z \sim 0.01$ nm and $\Delta v \sim 3.5\pi \times 10^3$ nm/s, which in reduced units gives $\sim 10^{-3}$ for both position and velocity. An inspection of Fig. 2 shows that those perturbations represent a negligible change in the tip oscillation.

Intrinsic perturbations are due to the finite time response of the feedback electronics, usually in the 10^{-4} s range. This implies that if the tip is laterally displaced at a speed of 10 μm/s, a topographic feature of arbitrary height (or depth) with a side slope of 60° would produce a maximum change of the rest tip-surface separation Δz_c of $\sim \pm 1.7$ nm before the feedback takes over. The perturbation will be followed by a transient and after that the tip will reach a stable (intermediate) oscillation. From there the feedback will smoothly reestablish the A_{sp} value. An AM-AFM will be operating properly if the intermediate and initial (unperturbed) states belong to the same branch, otherwise instabilities and image artifacts should appear.

A very small perturbation, $\Delta z_c = +0.1$ nm, is required to go from H to L at $z_c = 16$ nm. The converse change requires a perturbation of $\Delta z_c \sim -1.6$ nm. At $z_c = 14.5$ nm, the perturbation required to move from L to H is $+1.4$ nm, which coincides with the value needed to go from H to L. At $z_c = 7.5$ nm, the H state is very robust. *Intrinsic* perturbations of about -3.5 nm or $+7.5$ nm are needed to move from H to L. However, if the tip is in the L state, the minimum perturbation needed to move to the H branch is substantially smaller, $\Delta z_c \sim \pm 1.1$ nm. The above tendency reflects the changes in the repartition of the phase space between H and L basins of attraction as the separation is decreased.

We have performed measurements on InAs quantum dots grown by molecular beam epitaxy on a GaAs(001) substrate to test the predictions of the present model. First, we have determined the dependence of the amplitude on separation [Fig. 3(a)]. The plot shows the L and H branches (dots). However, the branches are incomplete. The upper and lower parts of H and L branches, respectively, are missing. For large separations the tip oscillates in state L. Decreasing the separation produces a sudden transition to the H state. From there on, the tip remains in the H oscillation state until the amplitude is zero. The missing sections of the branches correspond to a phase space which is dominated by the basin of attraction of the other state. The separation where the transition is observed may depend on the direction of the tip displacement (approaching/retracting). The direction of the tip displacement implies a different set of initial conditions for each separation. As a consequence, a small hysteresis loop in the amplitude curves may be observed if approaching/retracting cycles are performed.

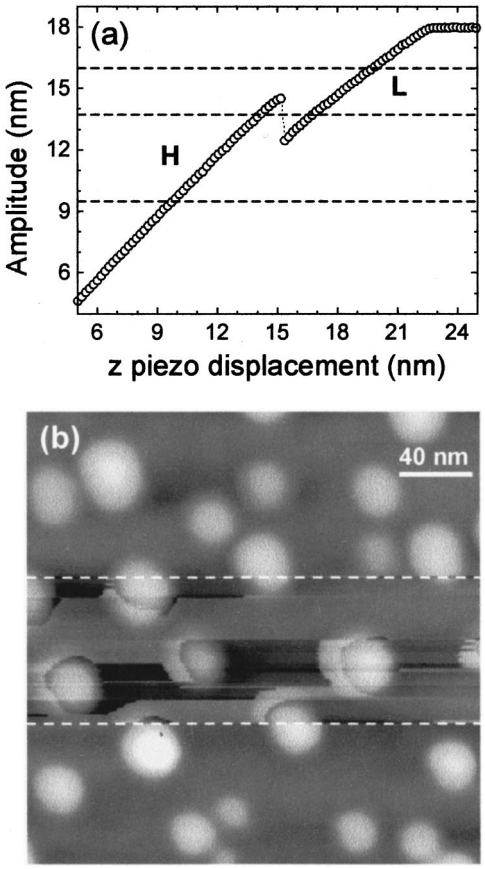

FIG. 3. Experimental determination of the low and high amplitude branches. (a) Amplitude curve, the L and H branches are plotted by open circles. Dashed lines indicate the A_{sp} values used to image a 200×200 nm^2 InAs quantum dot sample. (b) The system evolves from stable imaging in the L state $A_{sp} = 16$ nm (top), to unstable imaging due to switching between H and L states $A_{sp} = 13.8$ nm (middle), and finally to stable imaging in the H state $A_{sp} = 9.5$ nm (bottom).

The curve also shows a range of z positions, from 13 to 18 nm, where two different separations could give the same A_{sp}. The dashed lines indicate the A_{sp} values used to imaging the quantum dots shown in Fig. 3(b). Stable images are obtained for $A_{sp} = 16$ nm and $A_{sp} = 9.5$ nm, while a heavily distorted image is obtained at $A_{sp} = 13.8$ nm [Fig. 3(b)]. On the other hand, sudden topographic variations and dots surrounded by fringes are observed in the central region. Those features represent a vibrating tip switching between H and L states while scanning along the sample surface. Also in agreement with the model predictions, the switching between states only happens when (i) there is a substantial change of the topography, and (ii) the area of H and L basins of attractions are roughly the same.

It is an established practice in probe microscopy to attribute noisy or *unstable* data to a contaminated or bad tip shape. The role of an experienced observer to obtain faithful images is also acknowledged. A nonlinear dynamics analysis shows that in many cases noisy or unstable data only reflect the intrinsic structure of the tip motion. It also explains the manipulation of the observer with the driving frequency or

set point amplitude as a process that modifies the tip's phase space to reach a configuration where a single basin of attraction dominates the phase space projection. Additionally, it directs the experimental effort to select the state which minimizes tip-surface forces while optimizing spatial and compositional sensitivity.[24] Finally, there is a large amount of experimental data, for example, the single[25] and multiple[26] discontinuities observed in amplitude curves that can be readily interpreted as single or multiple transitions between high and low amplitude branches.

This work has been supported by the Dirección General de Investigación Científica y Técnica (PB98-0471) and the European Union (BICEPS, BIO4-CT-2112). A.S.P. acknowledges financial support from the Comunidad de Madrid.

[1] G. Binnig and H. Rohrer, Rev. Mod. Phys. **71**, 324 (1999); G. Binnig, C. Quate, and Ch. Gerber, Phys. Rev. Lett. **56**, 930 (1986).
[2] P. Hansma *et al.*, Appl. Phys. Lett. **64**, 1738 (1994).
[3] C. Bustamante and D. Keller, Phys. Today **48**, 33 (1995).
[4] F. J. Giessibl, Science **267**, 68 (1995).
[5] Y. Sugawara, M. Otha, H. Ueyama, and S. Morita, Science **270**, 1646 (1995).
[6] F. Ohnesorge, Surf. Interface Anal. **27**, 379 (1999).
[7] R. García, M. Calleja, and H. Rohrer, J. Appl. Phys. **86**, 1898 (1999).
[8] Y. Martin, C. C. Williams, and H. K. Wickramasinghe, J. Appl. Phys. **61**, 4723 (1987).
[9] T. R. Albrecht, P. Grütter, D. Horne, and D. Rugar, J. Appl. Phys. **69**, 668 (1991).
[10] S. N. Magonov, V. Elings, and M.-H. Whangbo, Surf. Sci. Lett. **375**, 385 (1997).
[11] F. Giessibl, Phys. Rev. B **56**, 16 010 (1997).
[12] P. Gleyzes, P. K. Kuo, and A. C. Boccara, Appl. Phys. Lett. **58**, 2989 (1991).
[13] B. Anczykowski, D. Krüger, and H. Fuchs, Phys. Rev. B **53**, 15 485 (1996).
[14] R. Boisgard, D. Michel, and J. P. Aimé, Surf. Sci. **401**, 199 (1998).
[15] R. García and A. San Paulo, Phys. Rev. B **60**, 4961 (1999).
[16] M. Marth, D. Maier, J. Honerkamp, R. Brandsch, and G. Bar, J. Appl. Phys. **85**, 7030 (1999).
[17] J. P. Aimé, R. Boisgard, L. Nony, and G. Courier, Phys. Rev. Lett. **82**, 3388 (1999).
[18] J. P. Hunt and D. Sarid, Appl. Phys. Lett. **72**, 2969 (1998); N. Sasaki, M. Tsukuda, R. Tamura, K. Abe, and N. Sato, Appl. Phys. A: Mater. Sci. Process. **66**, S287 (1998).
[19] B. V. Derjaguin, V. M. Muller, and Y. P. Toporov, J. Colloid Interface Sci. **53**, 314 (1975).
[20] W. Chin, E. Ott, H. E. Nusse, and C. Grebogi, Phys. Rev. E **50**, 4427 (1994).
[21] J. M. T. Thompson and H. B. Stwart, *Nonlinear Dynamics and Chaos* (John Wiley and Sons, New York, 1987).
[22] J. de Weger, D. Binks, J. Molenaar, and W. Van de Water, Phys. Rev. Lett. **76**, 3951 (1996).
[23] H.-J. Butt and M. Jaschke, Nanotechnology **6**, 1 (1995).
[24] A. San Paulo and R. García, Biophys. J. **78**, 1599 (2000).
[25] A. Kühle, A. H. Soerensen, and J. Bohr, J. Appl. Phys. **81**, 6562 (1997).
[26] G. Haugstad and R. Jones, Ultramicroscopy **76**, 77 (1999).